

Improving thermal state preparation of Sachdev-Ye-Kitaev model with reinforcement learning on quantum hardware

Akash Kundu

QTF Centre of Excellence, Department of Physics, University of Helsinki, Finland

Abstract

The Sachdev-Ye-Kitaev (SYK) model, known for its strong quantum correlations and chaotic behavior, serves as a key platform for quantum gravity studies. However, variationally preparing thermal states on near-term quantum processors for large systems ($N > 12$, where N is the number of Majorana fermions) presents a significant challenge due to the rapid growth in the complexity of parameterized quantum circuits. This paper addresses this challenge by integrating reinforcement learning (RL) with convolutional neural networks, employing an iterative approach to optimize the quantum circuit and its parameters. The refinement process is guided by a composite reward signal derived from entropy and the expectation values of the SYK Hamiltonian. This approach reduces the number of CNOT gates by two orders of magnitude for systems $N \geq 12$ compared to traditional methods like first-order Trotterization. We demonstrate the effectiveness of the RL framework in both noiseless and noisy quantum hardware environments, maintaining high accuracy in thermal state preparation. This work contributes to the advancement of a scalable, RL-based framework with applications for computations of thermal out-of-time-order correlators in quantum many-body systems and quantum gravity studies on near-term quantum hardware.

1 Introduction

The holographic duality [1] establishes a profound connection between a specific class of quantum field theories in d dimensions and quantum gravity in $d + 1$ dimensions. This strong/weak duality allows the exploration of strongly coupled field theories via classical supergravity and vice versa. Despite its power, there are no known cases where both sides of the duality can be simultaneously and analytically solved. The Sachdev-Ye-Kitaev (SYK) model, a simplified variant of the Sachdev-Ye model [2], was introduced in a series of seminal talks by Kitaev [3, 4]. This model exhibits holographic properties and is particularly amenable to study in the strong-coupling limit.

The SYK model consists of N Majorana fermions in $0 + 1$ dimensions with random couplings between q fermions, drawn from a Gaussian distribution with zero mean and variance proportional to J^2/N^{q-1} . In the large- N and low-temperature limit $N \gg \beta J \gg 1$, where β is the inverse temperature and J the disorder strength—the model displays an approximate conformal symmetry and is related to near-extremal black holes with a nAdS₂ (near-AdS₂) geometry. Meanwhile, the SYK model saturates the chaos bound [5], a key feature of holographic systems. Moreover, SYK model is a prominent example of a fast scrambler [6], known for its logarithmic growth of complexity and

its saturation of the bounds proposed by the Brown-Susskind conjecture regarding quantum information scrambling in black holes [7]. Its computational tractability in $0+1$ dimensions has enabled extensive numerical studies, with systems comprising up to 60 Majorana fermions analyzed [8, 9]. Over the past decade, the SYK model has been extensively studied in both condensed matter and high-energy physics [10, 11, 12]. For a comprehensive review, see refs. [13, 14, 15].

Given its significance in holography, detailed investigations of both pure and thermal (Gibbs) states of the SYK model are imperative. The ground state exhibits volume-law entanglement entropy with a known coefficient [16], rendering it classically challenging to prepare [17]. Additionally, a defining feature of the SYK model is the behavior of thermal four-point correlators, particularly out-of-time-order correlators (OTOCs), which saturate the Lyapunov exponent in the large- N and low-temperature regime [5]. Accurate computation of these OTOCs requires preparing the corresponding thermal state, which is a central focus of this study. While low-energy states have been explored via large-scale classical simulations, our research aims to advance the state-of-the-art by employing hybrid quantum-classical algorithms [18, 19].

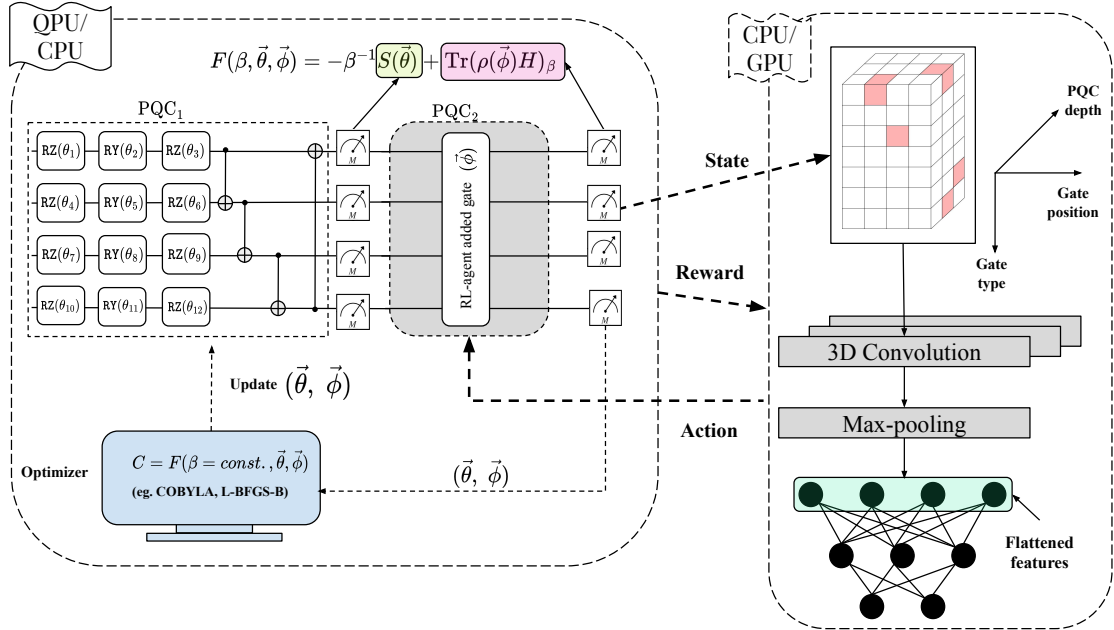


Figure 1: **Illustration of the main algorithm, where the environment, i.e., the PQC₂ in the variational framework encoded in a 3D tensor, interacts with an agent that is constructed using a 3D convolutional neural network under a reinforcement learning (RL) framework.** A classical optimizer optimizes the variational circuits and provides a reward signal to guide the agent in selecting subsequent actions. Upon receiving a reward and the current state s of the environment, the RL-agent chooses an action a in s in accordance with a ϵ -greedy policy. Using this framework, in Fig. 2 we show that the number of CNOT gates is reduced by 10^2 -fold beyond $N = 14$ Majorana fermions in PQC₂ compared to a first-order Trotter approximation.

Recent efforts have applied various quantum simulation techniques to the SYK model, including digital simulation [20], teleportation protocols [21], computation of bosonic correlation func-

tions [22], and ground-state preparation of coupled SYK models [23, 24]. Notably, ref. [25] employed a variational quantum algorithm to prepare thermal states of dense and sparse SYK models for $6 \leq N \leq 12$ Majorana fermions across a range of temperatures. Which is an extension of ref. [26], the authors focus on the real-time dynamics of the SYK model using quantum hardware. However, this approach faces significant challenges, including the rapid growth in the number of parameters and controlled-NOT (CNOT) gates with increasing N . These limitations restricted simulations to $N \leq 12$, as larger systems incurred prohibitive computational overhead.

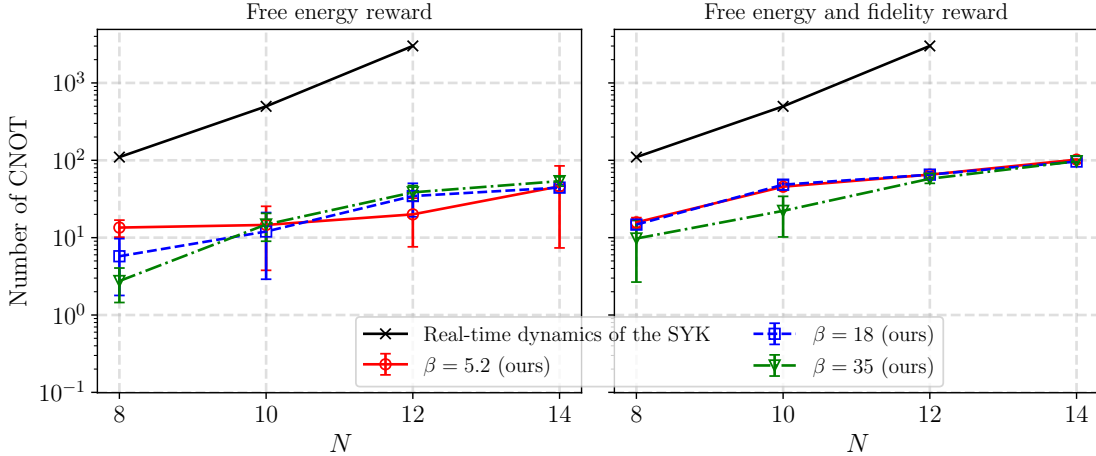


Figure 2: **The CNOT gates in the PQC_2 are 10^2 -fold improved beyond $N = 12$ if the thermal state is prepared in the reinforcement learning framework compared to the real-time dynamics obtained by a first-order Trotterization [26].** The resource count is obtained in a noiseless scenario where both the environment and the agent are noiseless. Using the reward signal presented in Eq. 4 (where the signal constitutes the error in free energy, hence “Free energy reward”) and in Eq. 5 (where the signal constitutes the error in free energy and the thermal state fidelity, hence the “Free energy and fidelity reward”) and for different temperatures ($1/\beta$). The “ours” denotes the variational thermal state preparation under the reinforcement learning framework in Fig. 1.

In this work, we address these challenges by integrating reinforcement learning (RL) with convolutional neural networks (CNNs) [27] into the variational quantum algorithm (VQA) framework. RL has recently emerged as a powerful tool for addressing quantum computing problems on near-term quantum devices [28, 29, 30, 31, 32, 33, 34]. In this approach, quantum circuits are modeled as sequences of actions governed by a trainable policy. The VQA cost function, independently optimized using a classical optimizer, provides periodic feedback that contributes to the final reward signal. This reward signal updates the policy, maximizing expected returns and guiding the selection of optimal actions for subsequent steps.

State-of-the-art RL-based approaches typically update the policy using the reward signal only after the VQA optimization is complete. In contrast, our algorithm, as illustrated in Fig. 1, employs a composite reward function updated iteratively. This reward function combines two key components: the entropy measured from the output of the first parameterized quantum circuit

(PQC₁)¹, and the expectation value of the SYK Hamiltonian computed after applying the second parameterized quantum circuit (PQC₂). Moreover, instead of frequently used feedforward neural networks (FNN) [35, 36] we utilize a 3D-CNN to enhance the trainability of the RL framework.

In essence, we train a CNN within a reinforcement learning framework using an ϵ -greedy policy guided by this composite reward signal in two different scenarios: (1) environment: noiseless, agent: noiseless up to $N = 14$ Majorana fermions; and (2) environment: noisy with constrained qubit connectivity, agent: noiseless for $N = 8$ Majorana fermions. The RL framework enables the identification of optimal parameterized quantum circuits for preparing thermal states across various temperatures, significantly reducing computational overhead. To demonstrate the effectiveness of the framework in Fig. 2 we summarize one of the main outcomes of the paper in scenario (1), which says that in a noiseless scenario, *compared to parameterized circuits obtained using real-time dynamics, i.e., the first-order Trotterization of the SYK Hamiltonian, our method (depicted in Fig. 1) reduces the number of CNOT gates at least by a factor of 10^2 when $N \geq 12$ while maintaining high accuracy in thermal state estimation over a wide temperature range.* We also demonstrate that the accuracy of thermal state preparation can be further enhanced by refining the reward function in the reinforcement learning process.

In scenario (2), the noiseless agent interacts with a noisy environment, where the entropy and the expectation value of the SYK Hamiltonian are computed in the presence of 1- and 2-qubit gate noise in PQC₁ and PQC₂. The qubits follow the constrained connectivity of the IBM **Eagle r3** processor. Our results indicate that for certain temperatures, the RL agent achieves better accuracy in the energy expectation value and entropy compared to scenario (1). However, when both quantities are combined to calculate the free energy, the accuracy degrades compared to the noiseless scenario. This can be tackled by utilizing sophisticated error mitigation techniques.

Finally, we evaluate the noise resilience of the parameterized circuits proposed by the RL agent by sampling the best-performing circuits from scenario (1) and running them on the IBM **Eagle r3** processor. Although the accuracy in the energy expectation value and entropy experiences a significant decrease due to noise in the QPU, its impact on the free energy is less pronounced.

The remainder of the sections is organized as follows: in Sec. 2 we elaborate on the preliminaries, such as the problem statement and the variational thermal state preparation algorithm. This is followed by an introduction to the variational preparation of the thermal states in the RL framework in Sec. 3. In Sec. 4 we thoroughly discuss the main results of the paper, including the efficiency of the RL framework in noiseless and realistic noisy scenarios. Finally in Sec. 5 we conclude the paper and discuss possible future work following the success of this paper.

2 Preliminaries

2.1 The problem: Dense SYK model

The Hamiltonian for the full or dense SYK model with N Majorana fermions and q -fermion interaction terms is:

$$H = \frac{\binom{i}{q}^{q/2}}{q!} \sum_{i,j,k,\dots,q=1}^N J_{i_1 i_2 \dots i_q} \chi_i \chi_j \chi_k \dots \chi_q, \quad (1)$$

where χ_i are Majorana fermions satisfying the anticommutation relation $\{\chi_i, \chi_j\} = \chi_i \chi_j + \chi_j \chi_i = \delta_{ij}$. We focus on the case where $q = 4$, which corresponds to random all-to-all quartic interactions

¹PQC₁ consists of a layer of RZ-RY-RZ gates on all qubits and all-to-all connected CNOT gates.

averaged over disorder. The random couplings $J_{i_1 i_2 i_3 i_4}$ are real-valued and are sampled from a Gaussian distribution with the following properties for the mean and variance:

$$\overline{J_{ijkl}} = 0, \quad \text{and} \quad \overline{J_{ijkl}^2} = \frac{3!J^2}{N^3}, \quad (2)$$

respectively. We set $J = 1$ in this work. The dimension of the Hilbert space is $\dim(\mathcal{H}) = 2^{N/2}$ where $n = N/2$ is the number of qubits is, we have $N = 2n$ since two Majorana fermions can be represented by one complex spinless fermion, which can be represented by a single qubit. The model can also be considered for $q > 4$ and is solvable in the large q limit [10]. However, here, we will restrict ourselves to the version given in Eq. (1) with $q = 4$. For this work, we choose dimensionless parameters and refer to βJ simply as β .

One of the challenges of the dense SYK model is that the number of terms in the Hamiltonian grows as $\sim N^4$. To reduce the computational cost of classical or quantum simulations of the SYK model, a sparsified version was introduced in Ref. [37, 38].

Due to the computational overhead of the dense SYK model and the rapidly increasing number of CNOT gates in the PQC₂ with increasing N , the authors in ref. [25] could not extend the task of thermal state preparation of the SYK model beyond 12 Majorana fermions using the variational quantum algorithm framework. We tackle this computational overhead by employing a reinforcement learning (RL) framework with an ϵ -greedy policy. Meanwhile, the RL agent is defined with a 3D convolutional neural network that takes a 3D tensor, encodes the quantum circuit as input.

2.2 Variational thermal state preparation

Thermal states, represented by a density matrix ρ_β , are critical for studying quantum systems at finite temperatures. These states are challenging to prepare compared to ground states ($\beta \rightarrow \infty$) or high-temperature states ($\beta \rightarrow 0$), which are computationally simpler. The finite inverse temperature regime (β) is particularly important for analyzing quantum many-body systems such as the SYK model.

To prepare a thermal state, we minimize the Helmholtz free energy F , given by

$$F = \langle H \rangle_\beta - TS_v, \quad (3)$$

where $T = 1/\beta$ is the temperature, $\langle H \rangle_\beta = \text{Tr}[\rho_\beta H]$ is the energy expectation value, where ρ_β is the thermal state at temperature T , and $S_v = -\text{Tr}[\rho_\beta \log \rho_\beta]$ is the von Neumann entropy. We adopt the algorithm from Ref. [39] whose subroutines are defined in the following.

Initialization: Begin with all qubits initialized in the state $|0\rangle^{\otimes n}$.

First variational circuit PQC₁²

- **Ansatz construction:** We utilize a hardware-efficient ansatz comprising layers of RZ-RY-RZ gates on each qubit, followed by CNOT entangling gates between qubits, as previously described by ref. [25]. This structure is chosen for its ease of implementation on real quantum hardware, offering a practical approach to circuit design.

²PQC₁ and PQC₁($\vec{\theta}$) are interchangeably used throughout the paper, but they carry the same meaning.

- **Measurement and entropy computation:** Apply the unitary transformation $\text{PQC}_1(\vec{\theta})$, where $\vec{\theta}$ are the variational parameters. The resulting quantum state is $|\psi(\vec{\theta})\rangle = \text{PQC}_1(\vec{\theta}) |0\rangle^{\otimes n}$. Then measure qubits in the computational basis and compute the Shannon entropy:

$$S = - \sum_{i=1}^{2^n} p_i(\vec{\theta}) \log p_i(\vec{\theta}),$$

where $p_i(\vec{\theta}) = |a_i(\vec{\theta})|^2$ represents the probability of the i^{th} basis state.

Second variational circuit (PQC_2): ³

- **Initialization:** Use the measurement outcome from PQC_1 as the initial state for PQC_2 .
- **Ansatz construction:** Employ a problem-specific or quantum hardware-inspired ansatz [40] with gates either derived from the trotterized time evolution operator or obtained from the native gateset from quantum hardware.
- **Thermal state approximation:** Apply the unitary transformation $\text{PQC}_2(\vec{\phi})$, where $\vec{\phi}$ are the variational parameters. Map the measured basis states to a superposition of orthonormal states. The final density matrix after PQC_2 is:

$$\rho_{\text{PQC}_2} = \sum_i |a_i(\vec{\theta})|^2 |\Psi_i(\vec{\phi})\rangle \langle \Psi_i(\vec{\phi})|,$$

where $|\Psi_i(\vec{\phi})\rangle = \text{PQC}_2(\vec{\phi}) |b_i\rangle$.

- **Free energy minimization:** Minimize the free energy $F = \langle H \rangle_{\beta} - TS$ using a classical optimizer to refine the parameters θ and ϕ .

Performance evaluation: Evaluate the free energy, entropy, and energy expectation value and compare with theoretical values.

3 Variational thermal state preparation with reinforcement learning

We give an overview of the variational thermal state preparation of the SYK model within the reinforcement learning (RL) framework, for details of the framework see Appendix A. The algorithm is illustrated in Fig. 1. The framework is used to estimate the parameters of the PQC_1 and the structure as well as parameters of the PQC_2 elaborated in Sec. 2.2. Wherein we present state, the action representations, and the reward function used in this work.

³ PQC_2 and $\text{PQC}_2(\vec{\phi})$ are interchangeably used throughout the paper, but they carry the same meaning.

The state In the hybrid quantum-classical environment, the agent begins each episode with PQC_1 (which includes a layer of RZ-RY-RZ rotations on each qubit followed by CNOT entangling gate), then it sequentially adds gates to the PQC_2 (which starts as an empty circuit at the beginning of each episode) until the maximum number of actions is reached. At each step, the state is represented by the current circuit, i.e., PQC_1 combined with PQC_2 , and the action is to append a gate. To enable deep RL methods, states and actions are encoded in a format suitable for neural networks. Specifically, each state is represented by a tensor-based binary encoding of the circuit’s gate structure, as described in Appendix B. The action space consists of CNOT gates and 1-qubit parameterized rotation gates (RX, RY, and RZ). Notably, we omit the continuous parameters of the rotation gates, focusing instead on the estimated energy of the circuit to define the state representation for the RL agent.

The agent The reinforcement learning (RL) agent utilizes a 3D convolutional neural network (CNN), as the quantum circuit is encoded as a 3D tensor (refer to Appendix B). In prior studies [29, 41, 28, 42], this 3D representation was typically flattened into a 1D format to be processed by a fully connected feedforward neural network (FNN) [35, 36]. However, flattening 3D data into 1D can result in the loss of critical spatial information, diminished model expressiveness, and potentially suboptimal performance. Architectures like 3D CNNs that can directly process the 3D structure are often preferable when working with volumetric data. If not flattened when operating on a structure like a 3D-CNN [43, 44], the neural net receives a dataset with distinguishable spatial information. In the case of the 3D binary encoding, where the X-axis represents the position of gates in PQC_2 , the Y-axis denotes the type of gate, and the Z-direction is the depth of PQC_2 . In Appendix C we elaborately show that directly feeding higher-dimensional data through a 3D-CNN provides improved training, leading to lower approximation error with more compact parameterized quantum circuits compared to processing flattened data through an FNN. The hyperparameters settings of the agent is discussed in Appendix F

The reward function To steer the agent towards the target, we use the same reward function r at every time step t of an episode, as in [31]. The reward function is r defined as

$$r = \begin{cases} 5, & \text{if } F_t(\beta = \text{const.}, \vec{\theta}, \vec{\phi}) < \zeta_F, \\ -5, & \text{if } F_t(\beta = \text{const.}, \vec{\theta}, \vec{\phi}) < \zeta_F \text{ and, step no.} = D_{\max}, \\ E_{\text{term}}, & \text{otherwise.} \end{cases} \quad (4)$$

Where $F_t(\beta = \text{const.}, \vec{\theta}, \vec{\phi})$ is the Helmholtz free energy at a constant temperature, at each step t , and $E_{\text{term}} = \max\left(\frac{F_{\text{prev}} - F_{\text{current}}}{|F_{\text{prev}} - F_{\text{true}}|}, -1, 1\right)$. The ζ_F is a user-defined threshold value on the error in estimating the free energy, and D_{\max} denotes the total number of steps allowed for an episode, which can also be understood as the maximum number of actions allowed per episode. Note that the extreme reward values ± 5 signal the end of an episode, leading to two stopping conditions: exceeding the threshold or reaching the maximum number of actions. For our task, we set the ζ_F to 10^{-2} .

In Sec. 4 we show that using the reward Eq. 4 we can achieve a very good approximation of to the free energy, but it cannot provide as good an approximation to the energy expectation of the SYK Hamiltonian and the entropy. Hence we engineer the reward signal to incorporate the accuracy of the prepared thermal state by calculating its fidelity from the target thermal state after

PQC₂. Hence the modified reward function is given by

$$r = \begin{cases} 5, & \text{if } F_t(\beta = \text{const.}, \vec{\theta}, \vec{\phi}) < \zeta_F \text{ and, } \text{Fid}(\rho(\vec{\phi})) \geq \zeta_{\text{Fid}}. \\ -5, & \text{if } \text{Fid}(\rho(\vec{\phi})) < \zeta_{\text{Fid}} \text{ and, } \text{step no.} = D_{\text{max}}, \\ 0.6 \times E_{\text{term}} + 0.4 \times \text{Fid}_{\text{term}}, & \text{otherwise,} \end{cases} \quad (5)$$

Where $\text{Fid}_{\text{term}} = 2 \times \text{Fid}(\rho(\vec{\phi})) - 1$, $\text{Fid}(\rho(\vec{\phi})) = \text{Tr}\left(\sqrt{\rho_\beta^{1/2} \rho(\vec{\phi}) \rho_\beta^{1/2}}\right)$ and ρ_β represents the density matrix that corresponds to the true thermal state. ζ_{Fid} is the user-defined threshold on fidelity, throughout the paper we choose $\zeta_{\text{Fid}} = 0.9$.

In the upcoming section, we will see that compared to the reward function Eq. 4 and Eq. 5 to the results obtained in ref. [25], in the Sec. 4 we achieve higher accuracy in the free energy, the entropy, and the energy of the thermal state.

4 Results

We employ a reinforcement learning (RL) agent-driven variational quantum thermal state algorithm introduced in Ref. [39]. For the dense SYK model, we consider the first circuit (PQC₁, which calculates the entropy) to be constructed using strongly entangling layers [45]. The second circuit (PQC₂ which calculates the expectation value) is built using the agent, as described also in the previous section. For the numerical simulations, we use QULACS [46] implementation in a hybrid CPU and GPU interface⁴

Throughout the paper we use the gradient-free optimizer COBYLA [47] with 10^3 iterations to optimize the parameters of the PQC₁ and the PQC₂. The RL framework is running for a maximum of 5×10^3 episodes the RL environment interacts with the agent for a predefined number of steps. Furthermore, the agent is optimized by the ADAM optimizer [48] with 10^{-3} learning rate. Further details of the RL-agent can be found in Appendix C and the environment that contains the tensor-based state and the reward function is elaborated in Section 3.

Sampling the best-performing circuits As discussed earlier, during the training of 5×10^3 episodes, the RL agent generates a class of parameterized quantum circuits with varying depths and gate counts, meeting predefined thresholds for free energy and fidelity. Selecting a specific circuit that accurately approximates the free energy, Hamiltonian energy expectation, and entropy is a challenging task. To streamline this process, we employ a filtering subroutine to identify the best-performing circuit. This filter applies a threshold on the errors, defined as:

$$\varepsilon = \Delta F + w_a \Delta \langle H \rangle_\beta + w_b \Delta S, \quad (6)$$

where ΔF represents the error in free energy, $\Delta \langle H \rangle_\beta$, scaled by the weight factor w_a , corresponds to the error in the Hamiltonian expectation, and ΔS , scaled by w_b , denotes the error in entropy. Among the circuits proposed by the RL agent, the one minimizing ε is selected as the best-performing candidate.

The parameters w_a and w_b are dependent on the reward function and the number of qubits. The parameter values used in the subsequent simulations are summarized below:

⁴CPU: AMD Rome and GPU: Nvidia Ampere A100.

1. **Free energy reward (Eq. 4):** For $N = 8, 10,$ and $12,$ we use $w_b = 0$ and $w_a = 0.5, 1.02,$ and $2,$ respectively. For $N = 14,$ the best-performing circuit is obtained with $w_a = 0$ and $w_b = 2.$
2. **Free energy and fidelity reward (Eq. 5):** For $N = 8, 10,$ and $12,$ we use $w_b = 0$ and $w_a = 0.8, 1.02,$ and $1.16,$ respectively. Similarly, for $N = 14,$ the optimal circuit is found with $w_a = 0$ and $w_b = 2.$

The objective of optimizing thermal state preparation by adjusting the entropy threshold w_b for the range $8 < N < 14$ arises from our analysis of small Majorana fermionic systems. In these systems, the various quantum circuit structures proposed by the RL-agent provide a good approximation to the entropy of the thermal state due to the relatively small system size. This contrasts with larger systems, where a trade-off in accuracy arises between free energy and Hamiltonian expectations.

After gathering results from the RL agent, we find that for $N = 10$ and $N = 12,$ it is important to slightly increase the weight associated with the filter of $\Delta\langle H \rangle_\beta.$ Since the primary goal of the RL agent is to optimize free energy, this adjustment helps improve the accuracy of the thermal state representation. However, for $N = 14,$ while the RL agent achieves a good approximation of free energy, we encounter limitations in entropy accuracy that become significant bottlenecks. To address this issue, we propose switching off the weight of $\Delta\langle H \rangle_\beta$ and instead applying equal weight to the entropy filter. This approach not only enhances the approximation of free energy but also reduces errors in both entropy and $\Delta\langle H \rangle_\beta.$

Overall, this post-processing step is crucial for refining our results and ensuring a more accurate representation of thermal states. In Appendix G we illustrate the impact of a wide range of the weights on the sampling of the best thermal state from all possible solutions proposed by the RL-agent.

4.1 Noiseless simulation

In Fig.3, we present the results for the dense SYK model simulations for $N = 8, 10$ Majorana fermions, the results are scaled up to $N = 14$ in Fig. 4. Each simulation was carried out for five instances, and to benchmark the performance of the RL framework, the agent was retrained for each instance. In each panel of Fig.3 and Fig. 4, we report the free energy, the expectation value of the Hamiltonian, and the entropy. The solid line represents the mean of the exact values, while the green (yellow) region indicates the 1σ (2σ) deviation from the mean. Red dots correspond to the performance of the RL-agent parameterized circuit optimized using the free energy error as a reward signal (Eq. 4). Meanwhile, blue crosses depict the performance of the RL circuit using both the free energy error and the fidelity of the thermal state as reward signals (see Eq. 5). The error bars indicate one standard deviation for the given number of model instances. For $8 \leq N \leq 12,$ the fidelity achieved was in the range $0.80 \leq F(\rho(\vec{\phi})) \leq 0.98,$ whereas for $N = 14,$ the fidelity decreased below 0.80 in the range $0.4 < F(\rho(\vec{\phi})) \leq 0.80.$

In the RL framework, the scaling of the number of gates required is substantially lower compared to the scaling in first-order Trotterization. This efficient scaling enables the preparation of thermal states for increasing numbers of Majorana fermions using a minimal number of 1- and 2-qubit gates. Consequently, this study achieves, for the first time, a variational preparation of thermal states for $N = 14$ Majorana fermions, demonstrating good agreement in estimating the free energy. Notably, at $\beta = 5.2,$ the RL agent provided the most accurate approximation of the free energy and expectation value compared to other temperatures.

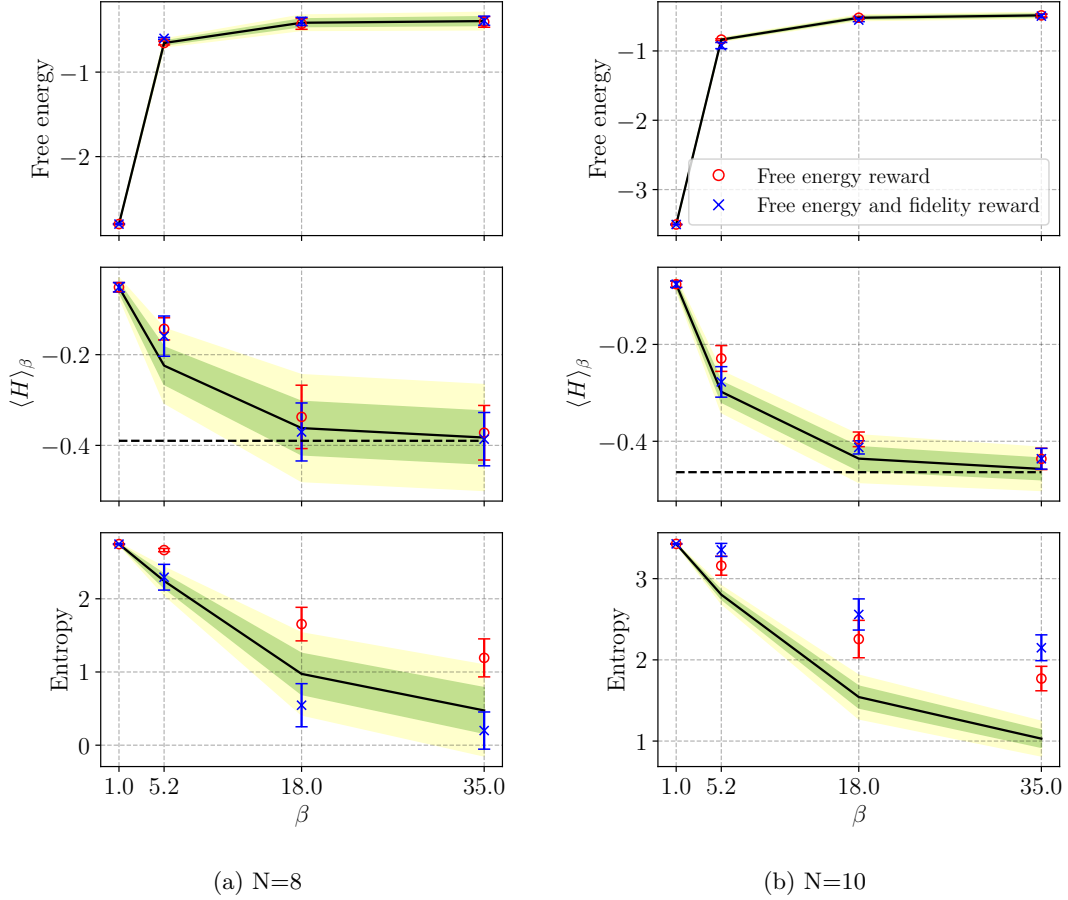


Figure 3: **RL framework enabling ground state preparation for $N = 8, 10$ Majorana fermions with high fidelity $F \geq 0.8$.** The number of gates required to achieve the result is at least 10-fold lower than the first-order Trotterized Hamiltonian-inspired ansatz for smaller systems. Red dots show RL-agent performance using free energy error as reward (Eq. 4). Blue crosses depict RL circuit performance using both free energy error and thermal state fidelity as rewards (Eq. 5). The solid line represents the exact mean, with green (yellow) regions indicating 1σ (2σ) deviations.

The noiseless simulation results exhibit very good agreement in the free energy, Hamiltonian expectation, and entropy for $N = 8$. However, as the number of Majorana fermions increases, the accuracy of the energy expectation and fidelity diminishes. Specifically, the error in estimating the Shannon entropy is significantly higher than the error in the Hamiltonian expectation value, although the free energy estimation error remains low.

Additionally, we observe that incorporating fidelity of the thermal state into the reward signal (blue crosses in Fig. 3 and Fig. 4) improves the accuracy of the energy expectation value. This improvement stems from the fidelity being evaluated alongside the expectation value immediately after executing PQC_2 . Enhanced fidelity in thermal state preparation directly improves the construction

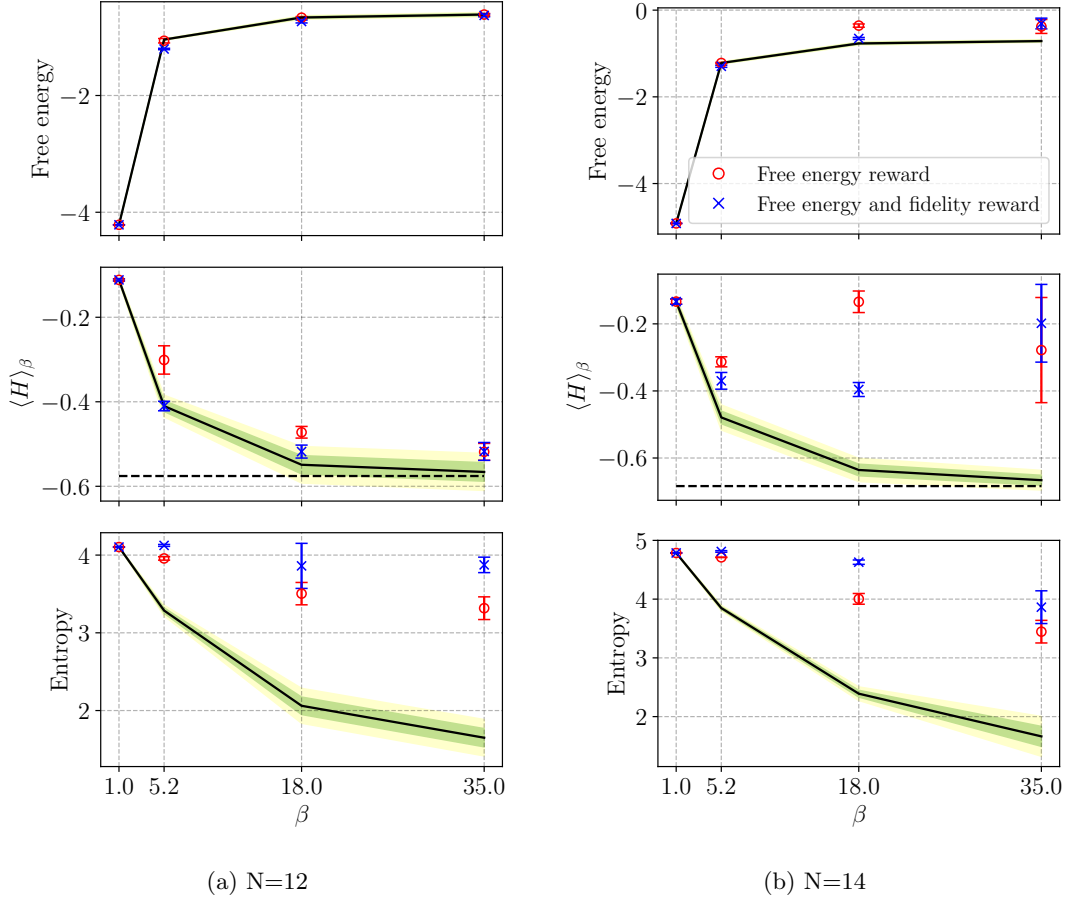


Figure 4: **RL framework surpasses the bottleneck in ref. [25], enabling ground state preparation for $N > 12$ Majorana fermions.** It achieves efficient gate scaling, facilitating thermal state preparation for $N \leq 14$ with fidelity $F \geq 0.8$ for $N = 12$. As stated in Fig. 3, Red dots show RL-agent performance using free energy error as reward (Eq. 4). Blue crosses depict RL circuit performance using both free energy error and thermal state fidelity as rewards (Eq. 5). The solid line represents the exact mean, with green (yellow) regions indicating 1σ (2σ) deviations.

of PQC_2 , thereby refining the accuracy of the Hamiltonian expectation value estimation.

In summary, the results highlight the effectiveness of the RL framework in variationally preparing thermal states when the system size scales. By incorporating fidelity into the reward mechanism, the RL approach achieves enhanced accuracy in energy expectation estimation, demonstrating its robustness and scalability. These findings encourage the exploration of the RL-driven quantum state preparation in noisy and hardware-contained scenarios.

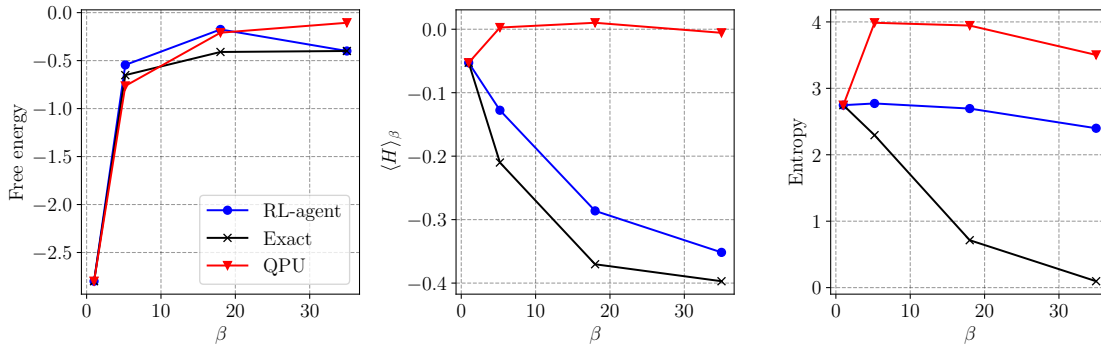


Figure 5: **The RL-agent selected circuit excels in approximating free energy for $N = 8$, even with hardware imperfections.** QPU noise significantly impacts Hamiltonian expectation value and entropy, yet free energy remains largely unaffected, demonstrating the RL-agent’s effectiveness in both ideal and noisy environments. This robustness suggests potential for training in realistic noisy conditions. No error-mitigation techniques were applied to the QPU.

4.2 Noise robustness on QPU

In this section, we study the robustness of the circuits selected by the RL-agent under realistic noisy conditions. The RL-agent is trained in a noiseless environment to optimize the parameterized circuits for minimizing the free energy. After training, the best circuit is selected according to how accurately it can find the free energy and then the circuit is executed on the IBM Eagle r3 processor to assess its practical performance. In the absence of any sophisticated error-mitigation techniques. See Appendix E for further information on the quantum hardware noise and limitations. The results were compared with exact classical calculations and experimental outcomes on the QPU for different temperatures.

Table 1: **Number of gates after transpilation on IBM Eagle r3 processor.**

To optimize	Gate type	$\beta = 5.2$	$\beta = 18$	$\beta = 35$
Entropy	1-qubit	63	69	59
	2-qubit	7	9	10
Expectation value	1-qubit	72	79	71
	2-qubit	9	10	10

Fig. 5 depicts the free energy, expectation value of the Hamiltonian, and entropy as functions of the inverse temperature β . The RL-selected circuit demonstrates good agreement with the exact theoretical results in the noiseless scenario. When deployed on the QPU, the error in the Hamiltonian expectation value and the entropy increase dramatically due to hardware imperfections, but the error in the free energy stays relatively lower and comparable to the noiseless scenario. This is because in this run the RL-agent is specifically trained to give a parameterized circuit that provides a proper approximation to the free energy, albeit the errors in the energy expectation value and the entropy are high. The number of gates after transpilation in the QPU is provided in

Tab. 1.

These results highlight the effectiveness of the RL-agent in identifying circuits that are not only optimal in idealized settings but also, to some extent, robust to QPU. The trade-off between accuracy and hardware limitations is evident, particularly at higher values of β , where noise effects become more pronounced. This tradeoff motivated us to train the agent in a realistic noisy environment imposed with the qubit connectivity constraints in the upcoming section.

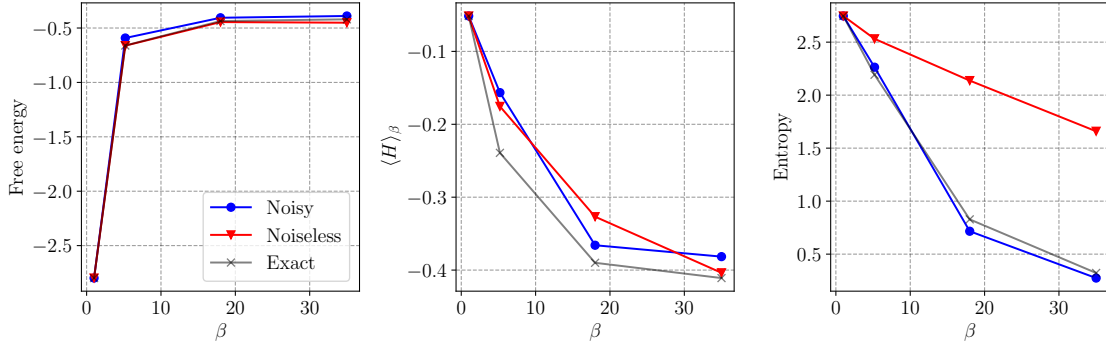


Figure 6: **Impact of noise and hardware connectivity constraints on thermal state preparation in the RL framework for $N = 8$ Majorana fermions.** The free energy accuracy decreases under realistic noise conditions (bit-flip and depolarizing noise), while the accuracy of the energy expectation value and entropy improves, showcasing the trade-offs introduced by noise in hardware-constrained quantum simulations.

4.3 Noisy training with constrained qubit connectivity

In this section, we consider the variational framework is noisy, i.e., each gate in the action space is subjected to quantum noise, leading to a noisy PQC_1 and PQC_2 where the noise values correspond to the median noise of `IBM_brisbane` device. As the action space consists of 1- and 2-qubit gates, we add bit flip noise of strength 2.342×10^{-4} after each application of a 1-qubit gate, and 2-qubit depolarizing noise of strength 8.043×10^{-3} is applied after each CNOT gate. Hence the RL agent interacts with a noisy environment and receives a noisy reward signal.

The results presented in Fig. 6 highlight the impact of noise during the simulation for $N = 8$ Majorana fermions, executed under the constrained connectivity of the `IBM Eagle r3` processor. A key observation is the improved accuracy of the energy expectation value and the entropy in the noisy scenario compared to the noiseless simulations. This improvement may be attributed to the adaptive optimization of the RL agent, which dynamically accounts for noise during the construction of the parameterized quantum circuit.

However, the cumulative accuracy of the free energy estimation diminishes noticeably in the presence of noise. This reduction is due to the cumulative effects of noise during the execution of the circuits. Unlike the energy expectation value and entropy, which are influenced by local noise-induced fluctuations, the free energy calculation depends on a more global accuracy of the thermal state, making it more susceptible to cumulative errors introduced by gate noise and connectivity constraints.

Hence, this leads us to conclude that the adaptive capabilities of the RL-agent allow for improved performance in certain metrics, such as energy expectation and entropy; the free energy is a more challenging quantity to optimize under realistic noise models. This analysis emphasizes the need for further enhancements in noise mitigation strategies [49, 50, 51, 52, 53].

4.4 Improvement in CNOT count

This section presents the improvement in the number of CNOT gates in the RL-agent proposed circuit compared to first-order Trotterization. The improvement is quantified by

$$\text{Improvement} = \frac{\text{CNOT}_{\text{trotterized}}}{\text{CNOT}_{\text{RL-agent}}}, \quad (7)$$

for different qubit counts and values of β . In Tab. 2 the results show that for 5 and 6 qubits, the RL-agent offers over a 10^2 -fold improvement in the number of CNOT gates compared to first-order Trotterization-based Hamiltonian variational ansatz [25], particularly for higher values of β . This demonstrates the ability of the RL-agent to significantly reduce circuit complexity as the qubit count increases, making it favorable for scaling to higher qubits.

Table 2: **Improvement in the number of CNOT gates in the RL-agent proposed circuit compared to first-order Trotterization.** The improvement is quantified as the ratio of the number of CNOT gates in the trotterized parameterized circuit to that in the RL-agent proposed circuit. On the **left**, we calculate the improvement using the free energy reward signal (as defined in Eq.4), while on the **right**, we consider the improvement with both free energy and fidelity as reward signals (as defined in Eq.5).

β	$N = 8$	$N = 10$	$N = 12$
5.2	32.7957	46.0322	242.7860
18	27.7726	54.7286	189.2048
35	84.6780	85.7093	349.0837

β	$N = 8$	$N = 10$	$N = 12$
5.2	46.1245	119.2494	571.6576
18	57.2831	68.1234	468.7002
35	15.5273	41.5346	406.7558

5 Conclusion and future work

Summary In this work, we present a novel approach to preparing thermal states of the Sachdev-Ye-Kitaev (SYK) model using a variational quantum algorithm in the reinforcement learning (RL) framework. In the variational algorithm, which plays the role of the environment in the RL framework, the parameterized quantum circuits are encoded in a 3D tensor. In the encoding, the X-axis represents the position of gates, the Y-axis denotes the type of gate, and the Z-direction is the depth. To process such higher-dimensional data, we integrate the environment with a 3D convolutional neural network (CNN) to optimize the preparation of the thermal states for different temperatures.

The 3D-CNN is guided by a ϵ -greedy policy, and a composite reward signal helps the agent to choose an action (i.e., a quantum gate) for a specific state of the environment. In this framework we operate in two key scenarios: (1) A fully noiseless environment for systems with up to $N = 14$ Majorana fermions. (2) A noisy environment with constrained qubit connectivity as per the IBM Eagle r3 processor for $N = 8$ Majorana fermions, using a noiseless agent.

This RL framework has proven highly effective in identifying optimal parameterized quantum circuits for thermal state preparation across a wide range of temperatures. Crucially, our approach

significantly reduces the computational overhead associated with this task, making it feasible to prepare thermal states for larger SYK systems, $N \geq 14$, which was previously not feasible. Our method significantly reduces the computational overhead associated with preparing thermal states for large SYK systems ($N > 12$ Majorana fermions) on near-term quantum devices. Key findings of the paper include:

1. A two order of magnitude reduction in the number of CNOT gates for systems $N \geq 12$ compared to traditional methods like first-order Trotterization.
2. Effective thermal state preparation in both noiseless and noisy quantum hardware environments, maintaining high accuracy.
3. Successful integration of reinforcement learning with convolutional neural networks to iteratively refine quantum circuits and their parameters.

This approach represents a significant advancement in RL-based quantum circuit optimization, with potential applications extending beyond the SYK model to broader quantum simulations and quantum gravity studies on near-term quantum hardware.

Future work Building on the success of this study, several promising directions for future research emerge:

1. **Scaling to larger systems:** Investigate the scalability of this approach for SYK models with $N > 14$ Majorana fermions, advancing the limits of current quantum simulations. This can be achieved by leveraging the recently proposed gadget reinforcement learning [54], which enables the learning of composite gate sets from smaller Majorana fermionic SYK models and subsequently applying them to solve models with a larger number of Majorana fermions efficiently.
2. **Out-of-time-order correlations:** Apply this method to accurately compute out-of-time-order correlations (OTOCs) for the SYK model, which are crucial for studying quantum chaos and holographic properties.
3. **Exploring reward engineering:** Explore other forms of reward function to benchmark the performance of the CNN agent. Such as we can encode the information corresponding to the properties of the thermal state (e.g., the entropy, purity, etc.) to improve the thermal state preparation further.
4. **Quantum information-theoretic analysis** Recent quantum informatic research suggests analyzing RL-agent-produced circuits can significantly enhance agent performance [55]. By applying quantum information-theoretic principles to circuit analysis, we can optimize circuit architectures, identify performance bottlenecks, and refine the RL framework’s efficiency.
5. **Advanced error mitigation:** Implement sophisticated error mitigation techniques such as [56, 50, 53, 57, 51] to improve the accuracy of results in noisy quantum environments, particularly for free energy calculations.
6. **Generalization to other models:** Extend the RL framework to optimize quantum circuits for other strongly correlated quantum systems beyond the SYK model.

6 Acknowledgment

The author expresses my gratitude to Sara Doelman for her insightful discussions on convolutional neural networks and her encouragement to publish these results. The author also thanks Raghav Govind Jha for the conversations that inspired this paper. Additionally, the author is grateful to Guilherme Ilário Correr, Aritra Sarkar, Abhishek Sadhu, Jarosław Adam Mischczak, and Stefano Mangini for their valuable suggestions and comments that improved the quality of this article. Finally, The author wish to acknowledge *CSC-IT Center for Science, Finland*, for computational resources.

References

- [1] Edward Witten. Anti de sitter space and holography. *arXiv preprint hep-th/9802150*, 1998.
- [2] Subir Sachdev and Jinwu Ye. Gapless spin-fluid ground state in a random quantum Heisenberg magnet. *Physical review letters*, 70(21):3339, 1993.
- [3] Alexei Kitaev. A simple model of quantum holography (part 1). *Entanglement in strongly-correlated quantum matter*, page 38, 2015.
- [4] Alexei Kitaev. A simple model of quantum holography (part 2). *Entanglement in strongly-correlated quantum matter*, page 38, 2015.
- [5] Juan Maldacena, Stephen H Shenker, and Douglas Stanford. A bound on chaos. *Journal of High Energy Physics*, 2016(8):1–17, 2016.
- [6] Jaewon Kim, Ehud Altman, and Xiangyu Cao. Dirac fast scramblers. *Physical Review B*, 103(8):L081113, 2021.
- [7] Adam R Brown, Leonard Susskind, and Ying Zhao. Quantum complexity and negative curvature. *Physical Review D*, 95(4):045010, 2017.
- [8] Guy Gur-Ari, Raghu Mahajan, and Abolhassan Vaezi. Does the SYK model have a spin glass phase? *Journal of High Energy Physics*, 2018(11):1–20, 2018.
- [9] Bryce Kobrin, Zhenbin Yang, Gregory D Kahanamoku-Meyer, Christopher T Olund, Joel E Moore, Douglas Stanford, and Norman Y Yao. Many-body chaos in the Sachdev-Ye-Kitaev model. *Physical review letters*, 126(3):030602, 2021.
- [10] Juan Maldacena and Douglas Stanford. Remarks on the Sachdev-Ye-Kitaev model. *Physical Review D*, 94(10):106002, 2016.
- [11] Joseph Polchinski and Vladimir Rosenhaus. The spectrum in the Sachdev-Ye-Kitaev model. *Journal of High Energy Physics*, 2016(4):1–25, 2016.
- [12] David J Gross and Vladimir Rosenhaus. A generalization of Sachdev-Ye-Kitaev. *Journal of High Energy Physics*, 2017(2):1–38, 2017.
- [13] Debanjan Chowdhury, Antoine Georges, Olivier Parcollet, and Subir Sachdev. Sachdev-Ye-Kitaev models and beyond: Window into non-fermi liquids. *Reviews of Modern Physics*, 94(3):035004, 2022.

- [14] Gábor Sárosi. Ads₂ holography and the SYK model. *arXiv preprint arXiv:1711.08482*, 2017.
- [15] Vladimir Rosenhaus. An introduction to the SYK model. *Journal of Physics A: Mathematical and Theoretical*, 52(32):323001, 2019.
- [16] Yichen Huang and Yingfei Gu. Eigenstate entanglement in the Sachdev-Ye-Kitaev model. *Physical Review D*, 100(4):041901, 2019.
- [17] Giacomo Passetti, Damian Hofmann, Pit Neitemeier, Lukas Grunwald, Michael A Sentef, and Dante M Kennes. Can neural quantum states learn volume-law ground states? *Physical Review Letters*, 131(3):036502, 2023.
- [18] Marco Cerezo, Andrew Arrasmith, Ryan Babbush, Simon C Benjamin, Suguru Endo, Keisuke Fujii, Jarrod R McClean, Kosuke Mitarai, Xiao Yuan, Lukasz Cincio, et al. Variational quantum algorithms. *Nature Reviews Physics*, 3(9):625–644, 2021.
- [19] Jarrod R McClean, Jonathan Romero, Ryan Babbush, and Alán Aspuru-Guzik. The theory of variational hybrid quantum-classical algorithms. *New Journal of Physics*, 18(2):023023, 2016.
- [20] Laura García-Álvarez, IL Egusquiza, Lucas Lamata, Adolfo Del Campo, Julian Sonner, and Enrique Solano. Digital quantum simulation of minimal ads/cft. *Physical review letters*, 119(4):040501, 2017.
- [21] Joseph D Lykken, Daniel Jafferis, Alexander Zlokapa, David K Kolchmeyer, Samantha I Davis, Hartmut Neven, and Maria Spiropulu. Long-range wormhole teleportation. *arXiv preprint arXiv:2405.07876*, 2024.
- [22] Zhihuang Luo, Yi-Zhuang You, Jun Li, Chao-Ming Jian, Dawei Lu, Cenke Xu, Bei Zeng, and Raymond Laflamme. Quantum simulation of the non-fermi-liquid state of Sachdev-Ye-Kitaev model. *npj Quantum Information*, 5(1):53, 2019.
- [23] Vincent Paul Su. Variational preparation of the Sachdev-Ye-Kitaev thermofield double. *arXiv preprint arXiv:2009.04488*, 2020.
- [24] Joonho Kim and Yaron Oz. Entanglement diagnostics for efficient quantum computation. *arXiv preprint arXiv:2102.12534*, 2021.
- [25] Jack Y Araz, Raghav G Jha, Felix Ringer, and Bharath Sambasivam. Thermal state preparation of the SYK model using a variational quantum algorithm. *arXiv preprint arXiv:2406.15545*, 2024.
- [26] Muhammad Asaduzzaman, Raghav G Jha, and Bharath Sambasivam. Sachdev-ye-kitaev model on a noisy quantum computer. *Physical Review D*, 109(10):105002, 2024.
- [27] Ian Goodfellow. *Deep learning*, 2016.
- [28] Yash J Patel, Akash Kundu, Mateusz Ostaszewski, Xavier Bonet-Monroig, Vedran Dunjko, and Onur Danaci. Curriculum reinforcement learning for quantum architecture search under hardware errors. In *The Twelfth International Conference on Learning Representations*.

- [29] Akash Kundu, Przemysław Bedelek, Mateusz Ostaszewski, Onur Danaci, Yash J Patel, Vedran Dunjko, and Jarosław A Mischczak. Enhancing variational quantum state diagonalization using reinforcement learning techniques. *New Journal of Physics*, 26(1):013034, 2024.
- [30] Yash J Patel, Sofiene Jerbi, Thomas Bäck, and Vedran Dunjko. Reinforcement learning assisted recursive QAOA. *EPJ Quantum Technology*, 11(1):6, 2024.
- [31] Mateusz Ostaszewski, Lea M Trenkwalder, Wojciech Masarczyk, Eleanor Scerri, and Vedran Dunjko. Reinforcement learning for optimization of variational quantum circuit architectures. *Advances in Neural Information Processing Systems*, 34:18182–18194, 2021.
- [32] En-Jui Kuo, Yao-Lung L Fang, and Samuel Yen-Chi Chen. Quantum architecture search via deep reinforcement learning. *arXiv preprint arXiv:2104.07715*, 2021.
- [33] Lorenzo Moro, Matteo GA Paris, Marcello Restelli, and Enrico Prati. Quantum compiling by deep reinforcement learning. *Communications Physics*, 4(1):178, 2021.
- [34] Paolo Andrea Erdman, Robert Czupryniak, Bibek Bhandari, Andrew N Jordan, Frank Noé, Jens Eisert, and Giacomo Guarnieri. Artificially intelligent maxwell’s demon for optimal control of open quantum systems. *arXiv preprint arXiv:2408.15328*, 2024.
- [35] Murat H Sazlı. A brief review of feed-forward neural networks. *Communications Faculty of Sciences University of Ankara Series A2-A3 Physical Sciences and Engineering*, 50(01), 2006.
- [36] Daniel Svozil, Vladimir Kvasnicka, and Jiri Pospichal. Introduction to multi-layer feed-forward neural networks. *Chemometrics and intelligent laboratory systems*, 39(1):43–62, 1997.
- [37] Antonio M García-García, Yiyang Jia, Dario Rosa, and Jacobus JM Verbaarschot. Sparse Sachdev-Ye-Kitaev model, quantum chaos, and gravity duals. *Physical Review D*, 103(10):106002, 2021.
- [38] Shenglong Xu, Leonard Susskind, Yuan Su, and Brian Swingle. A sparse model of quantum holography. *arXiv preprint arXiv:2008.02303*, 2020.
- [39] Johannes Selisko, Maximilian Amsler, Thomas Hammerschmidt, Ralf Drautz, and Thomas Eckl. Extending the variational quantum eigensolver to finite temperatures. *Quantum Science and Technology*, 9(1):015026, 2023.
- [40] Y Herasymenko and TE O’Brien. A diagrammatic approach to variational quantum ansatz construction. *Quantum*, 5:596, 2021.
- [41] Akash Kundu, Aritra Sarkar, and Abhishek Sadhu. KANQAS: Kolmogorov-Arnold network for quantum architecture search. *EPJ Quantum Technology*, 11(1):76, 2024.
- [42] Thomas Fösel, Murphy Yuezhen Niu, Florian Marquardt, and Li Li. Quantum circuit optimization with deep reinforcement learning. *arXiv preprint arXiv:2103.07585*, 2021.
- [43] Jonghoon Jin, Aysegül Dundar, and Eugenio Culurciello. Flattened convolutional neural networks for feedforward acceleration. *arXiv preprint arXiv:1412.5474*, 2014.
- [44] Delip Rao and Brian McMahan. *Natural language processing with PyTorch: build intelligent language applications using deep learning.* ” O’Reilly Media, Inc.”, 2019.

- [45] Maria Schuld, Alex Bocharov, Krysta M Svore, and Nathan Wiebe. Circuit-centric quantum classifiers. *Physical Review A*, 101(3):032308, 2020.
- [46] Yasunari Suzuki, Yoshiaki Kawase, Yuya Masumura, Yuria Hiraga, Masahiro Nakadai, Jiabao Chen, Ken M Nakanishi, Kosuke Mitarai, Ryosuke Imai, Shiro Tamiya, et al. Qulacs: a fast and versatile quantum circuit simulator for research purpose. *Quantum*, 5:559, 2021.
- [47] Michael JD Powell. A view of algorithms for optimization without derivatives. *Mathematics Today-Bulletin of the Institute of Mathematics and its Applications*, 43(5):170–174, 2007.
- [48] Diederik P Kingma. ADAM: A method for stochastic optimization. *arXiv preprint arXiv:1412.6980*, 2014.
- [49] Yuchen Guo and Shuo Yang. Quantum error mitigation via matrix product operators. *PRX Quantum*, 3(4):040313, 2022.
- [50] Sergei Filippov, Matea Leahy, Matteo AC Rossi, and Guillermo García-Pérez. Scalable tensor-network error mitigation for near-term quantum computing. *arXiv preprint arXiv:2307.11740*, 2023.
- [51] Ludmila Botelho, Adam Glos, Akash Kundu, Jarosław Adam Mischczak, Özlem Salehi, and Zoltán Zimborás. Error mitigation for variational quantum algorithms through mid-circuit measurements. *Physical Review A*, 105(2):022441, 2022.
- [52] Matteo Robbiati, Alejandro Sopena, Andrea Papaluca, and Stefano Carrazza. Real-time error mitigation for variational optimization on quantum hardware. *arXiv preprint arXiv:2311.05680*, 2023.
- [53] Zhenyu Cai, Ryan Babbush, Simon C Benjamin, Suguru Endo, William J Huggins, Ying Li, Jarrod R McClean, and Thomas E O’Brien. Quantum error mitigation. *Reviews of Modern Physics*, 95(4):045005, 2023.
- [54] Akash Kundu and Leopoldo Sarra. From easy to hard: Tackling quantum problems with learned gadgets for real hardware. *arXiv preprint arXiv:2411.00230*, 2024.
- [55] Abhishek Sadhu, Aritra Sarkar, and Akash Kundu. A quantum information theoretic analysis of reinforcement learning-assisted quantum architecture search. *Quantum Machine Intelligence*, 6(2):49, 2024.
- [56] Zhenyu Cai. Multi-exponential error extrapolation and combining error mitigation techniques for nisq applications. *npj Quantum Information*, 7(1):80, 2021.
- [57] Suguru Endo, Simon C Benjamin, and Ying Li. Practical quantum error mitigation for near-future applications. *Physical Review X*, 8(3):031027, 2018.
- [58] Richard S Sutton. Reinforcement learning: An introduction. *A Bradford Book*, 2018.
- [59] Hado Van Hasselt, Arthur Guez, and David Silver. Deep reinforcement learning with double q-learning. In *Proceedings of the AAAI conference on artificial intelligence*, volume 30, 2016.

- [60] Volodymyr Mnih, Koray Kavukcuoglu, David Silver, Andrei A Rusu, Joel Veness, Marc G Bellemare, Alex Graves, Martin Riedmiller, Andreas K Fidjeland, Georg Ostrovski, et al. Human-level control through deep reinforcement learning. *nature*, 518(7540):529–533, 2015.
- [61] Sparsh Mittal et al. A survey of accelerator architectures for 3d convolution neural networks. *Journal of Systems Architecture*, 115:102041, 2021.
- [62] Md Anwar Hossain and Md Shahriar Alam Sajib. Classification of image using convolutional neural network (CNN). *Global Journal of Computer Science and Technology*, 19(2):13–14, 2019.
- [63] Liang Zheng, Yali Zhao, Shengjin Wang, Jingdong Wang, and Qi Tian. Good practice in CNN feature transfer. *arXiv preprint arXiv:1604.00133*, 2016.
- [64] Maochang Zhu, Sheng Bin, and Gengxin Sun. Lite-3DCNN combined with attention mechanism for complex human movement recognition. *Computational Intelligence and Neuroscience*, 2022(1):4816549, 2022.
- [65] Zahid Ali Siddiqui and Unsang Park. Progressive convolutional neural network for incremental learning. *Electronics*, 10(16):1879, 2021.

A Reinforcement learning framework

In the context of Reinforcement Learning (RL), an agent interacts with its environment to learn an optimal policy through a process of trial and error [58]. This interaction can be formally modeled as a Markov Decision Process (MDP), defined by the tuple (S, A, P, R) , where:

- S represents the state space
- A represents the action space
- $P : S \times S \times A \rightarrow [0, 1]$ defines the transition dynamics
- $R : S \times A \rightarrow \mathbb{R}$ describes the reward function of the environment

In our work, we consider both the action space A and the state space S to be finite and discrete sets.

Agent behavior and performance metrics The agent’s behavior within the environment is governed by a stochastic policy $\pi(a|s) : S \times A \rightarrow [0, 1]$, where $a \in A$ and $s \in S$. To assess the agent’s performance, we use a metric called the *return*, which is calculated as a discounted sum:

$$G(\tau) = \sum_{j=0}^{T-1} r_j \gamma^{j+1} \tag{8}$$

Here, $\tau = (s_0, a_0, r_0, \dots, s_{T-1}, a_{T-1}, r_{T-1}) \in (S \times A \times \mathbb{R})^T$ represents the interaction sequence T is a fixed length called the horizon, and γ is an environment-specific discount factor. The primary objective of the agent is to determine the optimal policy that maximizes the expected return.

Function approximation and algorithm choice To handle large, unknown environments where the agent must adapt to various situations and develop multiple strategies simultaneously, we employ highly expressive function approximations. Specifically, we use deep neural networks to parametrize the agent’s policy π .

For our implementation, we have chosen to use a Double Deep Q-Network (DDQN) [59], which is an extension of the standard Deep Q-Network (DQN) [60]. The DDQN algorithm utilizes two neural networks to enhance the stability of Q-value predictions for each state-action pair.

State and action space representation In our specific application:

- The state space is represented as an ordered list of layers, each composed of a single depth of the quantum circuit.
- The action space is defined by a list of four numbers, corresponding to the quantum gates RX, RY, RZ, and CNOT.

B Tensor-based encoding of quantum circuits

We adopt a binary encoding scheme, as introduced in [28, 29], to capture the structure of PQC_2 , focusing on the order and arrangement of gates to provide the agent with a complete circuit description. Unlike previous approaches, which flattened the 3D encoding into one dimension for use in feedforward neural networks, our method leverages the full spatial structure of the encoding by employing a 3D convolutional neural network (CNN). This allows us to extract richer spatial features from the encoded representation as shown in the Appendix C. .

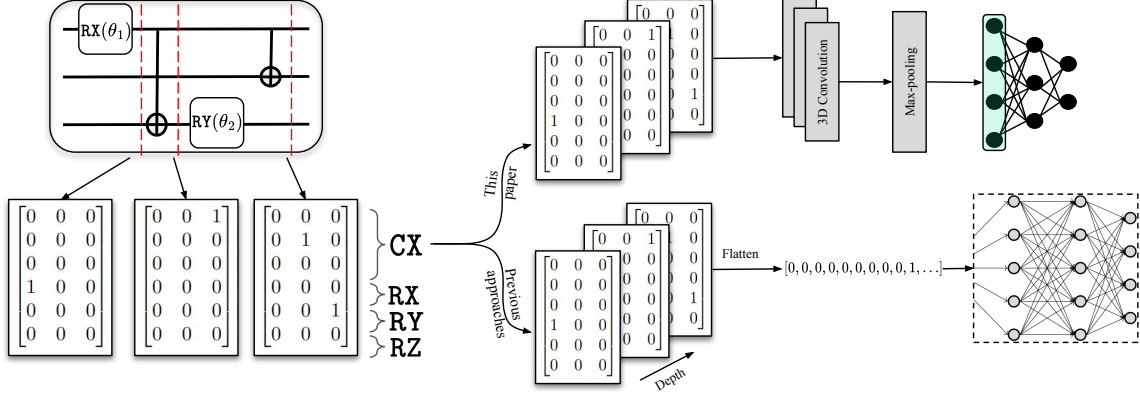


Figure 7: **The 3D tensor encoding of the PQC_2 circuit structure.** The representation captures gate number, order, and arrangement, enabling the use of 3D-CNN for richer spatial feature extraction, in contrast to flattened 1D encodings used with feedforward networks in previous approaches.

To construct the tensor encoding, we first define the hyperparameter D_{\max} , which sets the maximum number of allowed gates (or actions) in an episode. A *moment* in a PQC corresponds to all gates that can be executed simultaneously, thereby defining the circuit’s depth.

The PQCs are represented as 3D tensors initialized at each episode with an empty circuit of depth D_{\max} . This tensor has dimensions $[D_{\max} \times ((N + N_{1q}) \times N)]$, where N represents the number of qubits, and N_{1q} denotes the number of single-qubit gates. Each slice of the tensor has N rows for the control and target qubit positions of CNOT gates, followed by rows indicating the positions of single-qubit gates. For instance, as shown in Fig. 7, there are 3 rows for three spatial rotations, RX, RY and RZ.

C CNN outperforms FNN

We utilize 3D convolution, whose theory can be found elaborately in [61, 27]. One layer of 3D-CNN is defined as

Listing 1: One layer of 3D-CNN

```
for channel in channels_list:
    layer_list.append(Conv3d(input_channel, channel, kernel_size=(3,3,3), stride=(1,1,1),
        padding=(1,1,1)))
    layer_list.append(LeakyReLU())
    layer_list.append(MaxPool3d(kernel_size=(1,1,1), stride=(2,2,2), padding=0,
        dilation=1))
    input_channel = channel
```

In tackling the $N = 8$ SYK Hamiltonian, we consider `channels_list` in 1 as follows. For (1) *4 layers*: [32, 64, 128, 256], for (2) *5 layers*: [32, 64, 128, 256, 512], for (3) *6 layers*: [32, 64, 128, 256, 512, 1024] and for (4) *7 layers*: [32, 64, 128, 256, 512, 1024, 2048].

Following the standard approach in convolutional neural networks [62, 63, 64, 65], the architecture presented progressively increases the number of channels. Starting from 32 channels and doubling them at each layer. This is a common strategy to capture more intricate patterns in the data, which allows the network to learn increasingly complex features at deeper layers. The initial layers capture low-level features, while deeper layers capture high-level features. In the language of quantum architecture search the input to the 3DCNN is comprised of a 3D tensor whose axes represent quantum circuit depth, type of gates in the circuit, and the number of qubits; the object of the quantum circuit is to find the ground state of Hamiltonian. Hence the low-level features are defined by the depth, number of gates, and the number of qubits in the circuit, whereas the high-level feature is represented by the combinations of gates in the circuit, the performance metrics such as the objective function, and the reward received from the environment. Hence, increasing the layer of the 3D-CNN not only helps optimize the depth and the number of gates of the circuit using the first few layers, but the network makes sure that these circuits successfully reach the ground truth.

Whereas one-layer of 1D FNN is defined as:

Listing 2: One layer of FNN

```
for input_n, output_n in zip(neuron_list[:-1], neuron_list[1:]):
    layer_list.append(nn.Linear(input_n, output_n))
    layer_list.append(nn.LeakyReLU())
    layer_list.append(nn.Dropout(p=p))
```

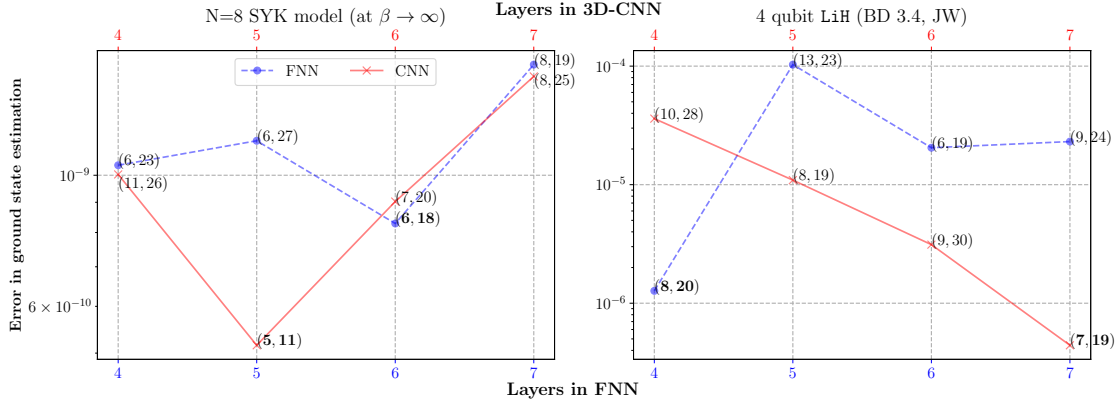


Figure 8: **Convolutional neural network (CNN) achieves a lower error in finding the ground state of the SYK model at $N = 8$ and finding the ground state of LiH molecule compared to feedforward neural network (FNN).** Along with $N = 8$ SYK Hamiltonian, we consider a well-known LiH chemical Hamiltonian to show the advantages of utilizing CNN over FNN in the RL framework. In the plot, by (a, b) we represent a CNOT and b 1-qubit rotations (i.e., total number of R_X , R_Y and R_Z). The CNN not only achieved much lower error in comparison to the FNN but did it with a fewer number of 1- and 2-qubit gates for both the problems.

In tackling the $N = 8$ SYK Hamiltonian, we consider `channels_list` in 2 as follows. For (1) 4 layers: [1000, 1000, 1000, 1000], for (2) 5 layers: [1000, 1000, 1000, 1000, 1000], for (3) 6 layers: [1000, 1000, 1000, 1000, 1000, 1000] and for (4) 7 layers: [1000, 1000, 1000, 1000, 1000, 1000, 1000].

D Resource quantization

Majorana fermions (N)	8	10	12	14
Time (in hours)	3.9162	24.2600	47.4669	47.8951

Table 3: **The RL-agent training time** to obtain the results presented in Sec. 4 for various number of Majorana fermions.

E The IBM Eagle r3 processor

The free energy and the entropy is calculated on `ibm.kyiv`, `ibm.sherbrooke` and `ibm.brisbane`. They are all 127 qubit devices with the **Eagle r3** processor. The qubit connectivity of these devices is shown in Fig. 9. All these machines use the same set of basis gates, which consist of ECR and single-qubit gates ID , RZ , SX , X .

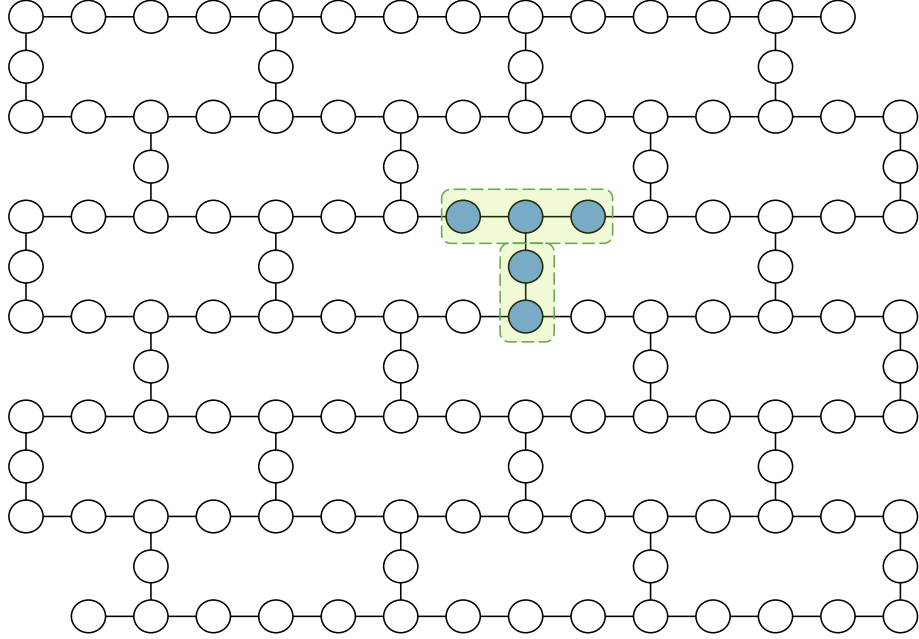


Figure 9: **Topology of the 127-qubit IBM Eagle r3 processors used in noisy experiments.** As we run the SYK Hamiltonian for $N = 8$ Majorana fermions, in the highlighted part of the topology we show that in this experiment we utilized a T-configuration that minimizes additional SWAP gates required due to the restricted connectivity of physical qubits as noted in ref. [26].

F The agent and environment hyperparameters

The hyperparameter tuning of the reinforcement learning agent corresponds to the tuning of the following parameters:

Batch size	Memory size	Dropout	Update target net	Final γ	ϵ decay	ϵ min	ϵ restart
10^3	2×10^4	0	500	5×10^{-3}	0.99995	5×10^{-2}	1

Table 4: The hyperparameters of the reinforcement learning agent.

1. Batch size: The number of experiences sampled from the memory for each training step.
2. Memory size: The total capacity of the experience replay buffer storing past interactions.
3. Dropout: The probability of randomly disabling neurons during training to prevent overfitting.
4. Update target net: The frequency (in steps) at which the target network is updated with the online network’s weights.
5. Final γ : The discount factor determining the importance of future rewards compared to immediate rewards.

6. ϵ : The rate at which the exploration probability decreases in the ϵ -greedy policy.
7. ϵ min: The minimum value of ϵ , ensuring a baseline level of exploration.
8. ϵ restart: The initial value of ϵ at the start of training or after a reset, representing the maximum exploration level.

G The art of sampling best circuits

The process of selecting optimal quantum circuits from those proposed by the Reinforcement Learning (RL) agent involves a filtering threshold defined as:

$$\varepsilon = \Delta F + w_a \Delta \langle H \rangle_\beta + w_b \Delta S, \quad (9)$$

where ΔF , $\Delta \langle H \rangle_\beta$, and ΔS represent errors in free energy, Hamiltonian expectation, and entropy, respectively. Weights w_a and w_b adjust the relative importance of these errors. The best-performing circuit is selected by:

1. Evaluating each proposed circuit using ε .
2. Selecting the circuit that minimizes ε .

Figures 10 and 11 illustrate the significant impact of weight selection on circuit sampling. These results emphasize the critical nature of careful postprocessing to achieve an optimal balance between free energy, Hamiltonian expectation value, and entropy of the thermal state. The findings underscore the importance of thoughtful parameter selection in the filtering process, as it directly influences the quality of the sampled circuits. This approach allows for fine-tuning the selection criteria to meet specific performance requirements in quantum circuit design and optimization.

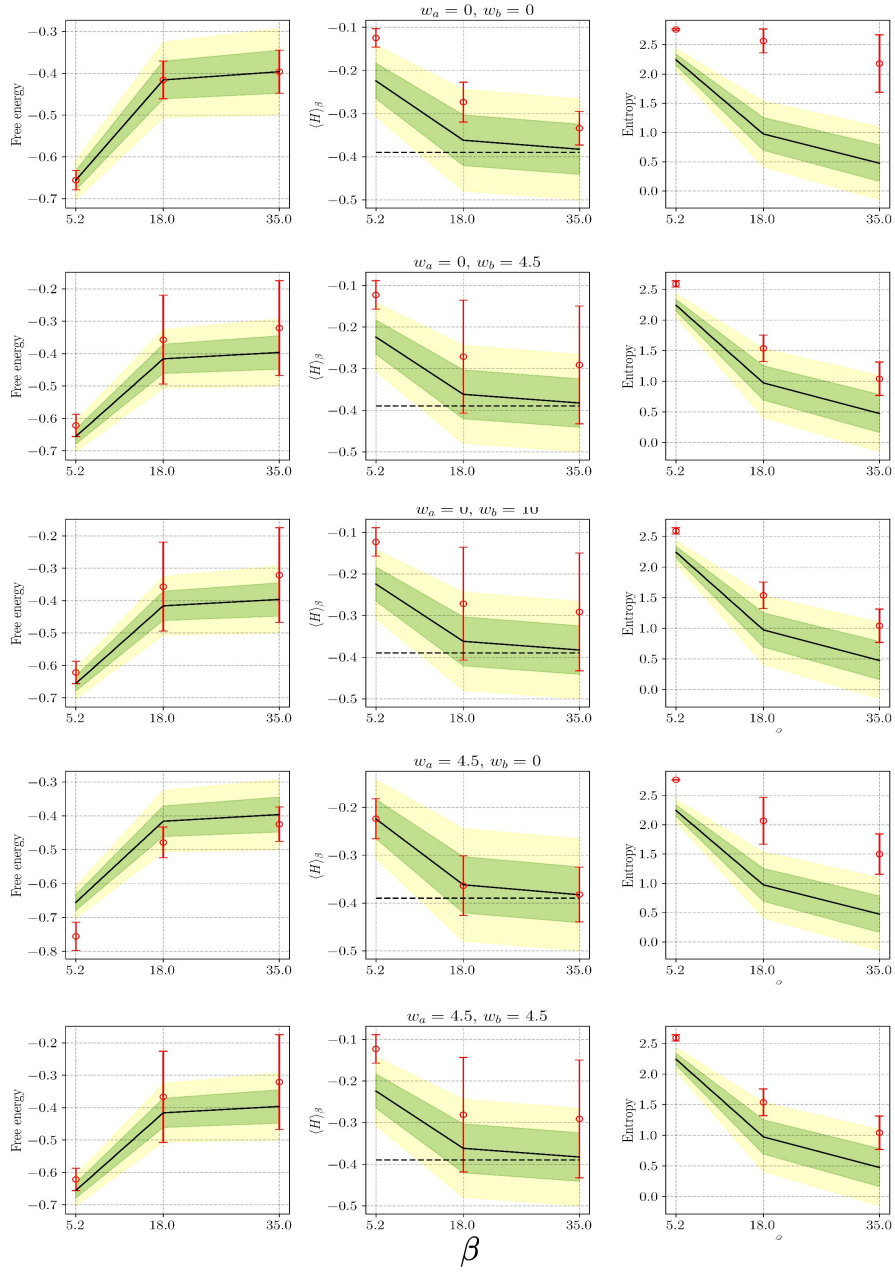


Figure 10: **Impact of the weights in the filtering threshold in Eq. 6 on the sampling of thermal states.** RL-agent proposes many possible structures of PQC_2 and it is important to find a tradeoff in the weight values to sample the best thermal state.

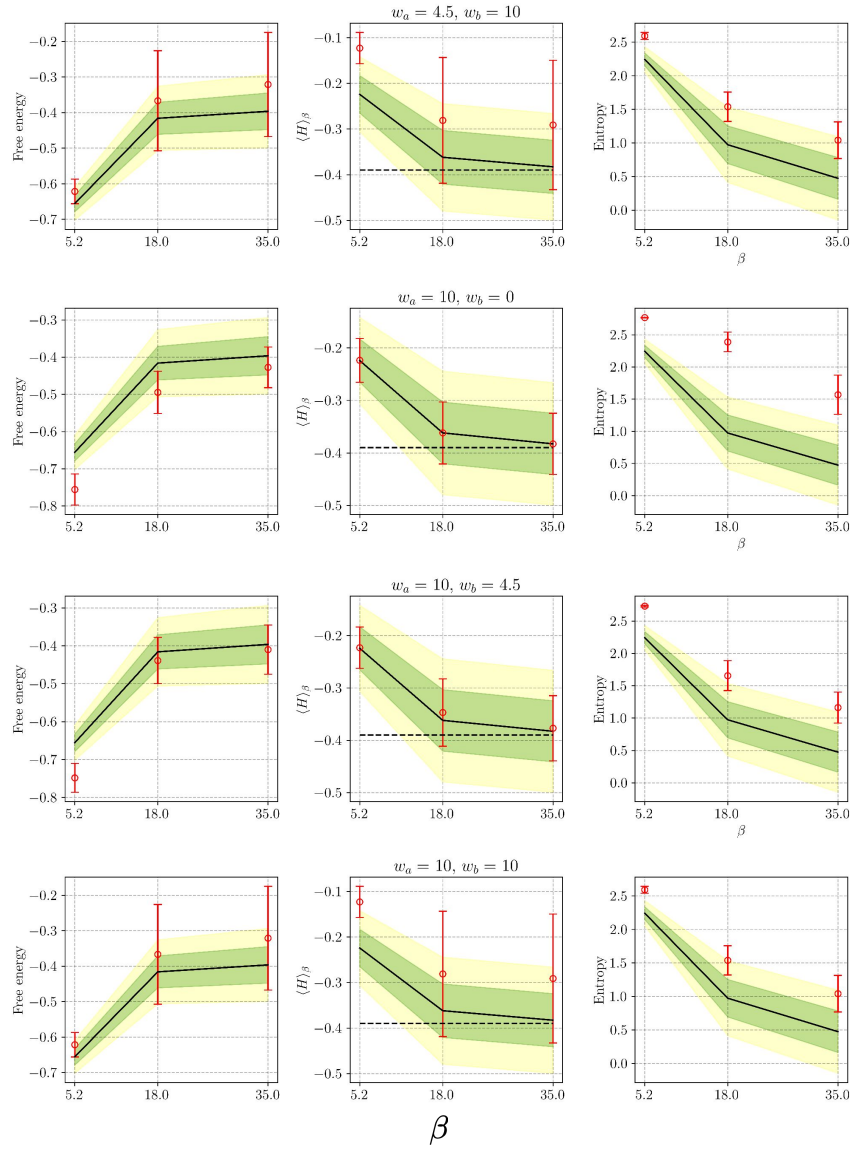


Figure 11: Impact of a wider range of weights in the filtering threshold in Eq. 6 on the sampling of thermal states. Continuation of the results in Fig. 11 for more weight values.